





Direct anodization–reduction nanomodification of gold films: investigating electrocatalysis of the emerging contaminant halobenzoquinone

José Antônio de Oliveira Júnior¹, Gilvana Pereira Siqueira¹, Lara Kelly Ribeiro², Dyovani Coelho², Elson Longo², André Mourão Batista⁴, Heinz-Bernhard Kraatz⁶, Auro Atsushi Tanaka^{1,3}, Luiza Maria Ferreira Dantas⁵, Marco Aurélio Suller Garcia^{1,*} , and Iranaldo Santos da Silva⁵ 

¹Departamento de Química, Universidade Federal do Maranhão, Avenida dos Portugueses 1966, São Luís, MA 65080-805, Brazil

²Departamento de Química, CDMF-UFSCar, Universidade Federal de São Carlos, Rod. Washington Luiz km 235, São Carlos, SP 13565-905, Brazil

³Instituto Nacional de Ciência e Tecnologia de Bioanalítica, Caixa Postal 6154, Campinas, SP 13083-970, Brazil

⁴Programa de Pós Graduação em Nanociências e Materiais Avançados, Universidade Federal do ABC, Avenida dos Estados 5001, Santo André, SP, Brazil

⁵Departamento de Tecnologia Química, Centro de Ciências Exatas e Tecnologia, Universidade Federal do Maranhão, São Luís, MA 65080-805, Brazil

⁶Department of Physical and Environmental Sciences, University of Toronto Scarborough, 1265 Military Trail, Toronto, ON M1C 1A4, Canada

Received: 29 July 2021

Accepted: 9 October 2021

Published online:

3 January 2022

© The Author(s), under exclusive licence to Springer Science+Business Media, LLC, part of Springer Nature 2021

ABSTRACT

Controlling the sensitivity, quantification, and detection limits of electrochemical sensors is an ongoing challenge. The properties of thin modified gold-film electrodes under varying potentials have been studied to improve such analytical validation parameters; however, most international literature on the subject tends to analyze the role of synthesis lonely without deep evaluating surface properties throughout every step of a modification process. Herein, we aimed to link materials science with sensing analytical application, revisiting a nanoporous gold-film electrochemical synthesis, and explain its performance using SEM, AFM, and XPS analyses. Also, we used the neglected emerging contaminant 2,6-dichloro-1,4-benzoquinone (DCBQ) for our analytical issues assessment. We were able to show the electrocatalytic effect of the prepared electrode, commonly mistreated in such field; also, we evaluated the sensor's modification for a possible explanation for the system's reproducibility (10 times without loss of activity, RSD inferior to 5%). Although the modification time presented an effect on the nanoporous electrode response, we could confirm

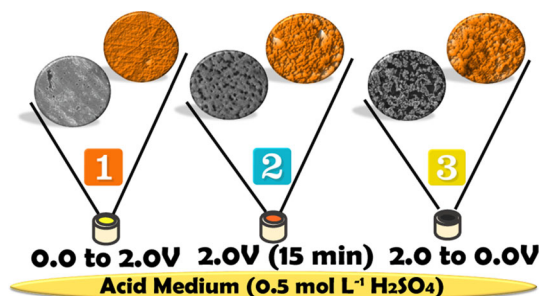
Handling Editor: Joshua Tong.

Address correspondence to E-mail: marco.suller@ufma.br

E-mail Address: iranaldo.ss@ufma.br

that it was not an area augmentation effect only based on the electrochemical characterizations. We believe we took a step forward to understand the effect of the electrochemical modification performed, which can be carried out in other systems, helping a more rational design of sensors.

GRAPHICAL ABSTRACT



Introduction

The properties of nanostructured materials—such as high surface area, quantum effects, and reactive capacity—are vital for the design of sensing devices [1, 2]. Based on these properties, nanotechnology techniques allow the rational optimization and design of materials with tunable behavior [3–6]. In this context, nanoporous gold electrodes (NPGEs) have gained a lot of attention once simple electrochemical approaches can be used for their preparation [7, 8]. Essentially, the electrochemical process avoids the need for capping ligands or other growth-directing agents, often required by nanometal or oxide synthesis, which can be detrimental as it may block active sites [9–11]. Conveniently accessible from bulk electrode materials, electrochemical strategies modifications generate materials with three-dimensional (3D) nanostructured porosity [12], possessing interesting properties as a result of additional adsorption and active sites compared to bulk electrodes [13].

Nanostructured sensor materials tend to preserve their structure and performance even for extended periods of operation [14]. And while gold-based nanoporous sensors have been reported in the literature [15–18], there is a lack of studies that focus on

relating the material's physicochemical characteristics with the electrochemical properties of the electrode. However, there is a fundamental need to gain more insight into this aspect to improve the performance of these sensor materials. Specific questions to be addressed are related to the role of surface modifications and their part on potential structural changes, also effects on the performance of the sensor material, including long-term performance. It is noticeable from the literature that 3D nanostructured gold electrodes prepared from bulk gold electrodes (GE) display enhanced performance for electrochemical sensing applications, which is interesting for detecting several potential environmental hazardous molecules [19, 20].

Herein, we describe the results of our studies into electrochemical nanomodification of gold electrodes and highlight the effects of (a) mechanical polishing of the unmodified electrode; (2) anodization at 2.00 V, held for 15 min; (3) electrochemical reduction to 0.00 V; both stages (2) and (3) were performed in acidic medium. Experimental evidence of morphological changes that occur during polarization and nanostructuring is provided by atomic force microscopy (AFM), and scanning electron microscopy (SEM), as well as additional spectroscopic data are provided (XPS) together with a detailed electrochemical characterization. We are using DCBQ as a

sample analyte, followed by a full evaluation of any changes in the surface morphology after each analytical cycle, including the sensor's performance after exhaustive repetitive measurements.

Experimental

Reagents

All chemicals were purchased from Sigma-Aldrich/Merck in analytical grade and were used without further purification and maintained at room temperature ($\sim 25\text{ }^{\circ}\text{C}$). The solutions were prepared with deionized water (resistivity of $18.20\text{ M}\Omega\text{ cm}$, Millipore®, Billerica, USA). An aqueous solution of $0.50\text{ mol L}^{-1}\text{ H}_2\text{SO}_4$ was used as a supporting electrolyte to prepare the NPGE. Standard DCBQ stocks (Sigma-Aldrich, St. Louis, MO) were prepared with ethanol 98% before measurements at different concentrations, and kept in the dark to avoid degradation.

Britton–Robinson (BR), citrate, acetate, and phosphate buffer solutions were used as support electrolytes in analytical measurements. The BR buffer (pH 3.00–8.00) was prepared from a mixture of acetic acid, boric acid, and phosphoric acid at a concentration ratio of 1:1:1 (0.10 mol L^{-1} each), with the addition of $3.00\text{ mol L}^{-1}\text{ NaOH}$ to adjust the pH medium. Other buffer solutions were made by adding $3.00\text{ mol L}^{-1}\text{ NaOH}$ to the acid solutions (citric, phosphoric, and acetic acids) with a 0.10 mol L^{-1} concentration. Lastly, a $5.00\text{ mmol L}^{-1}\text{ KCl}$ solution was made upon adding the salt to the desired volume of deionized water.

NPGE preparation

Before any measurement or modification, both GE and NPGE were polished mechanically using aluminum suspensions of various particle sizes (0.05 , 0.30 , 1.00 , and $3.00\text{ }\mu\text{m}$), after which they were cleansed with multiple washes in running deionized water. The NPGE used herein was prepared according to an anodization–reduction method described elsewhere with modifications [21]. For the modification, the potential was scanned from 0.00 to 2.00 V in $0.50\text{ mol L}^{-1}\text{ H}_2\text{SO}_4$ at a scan rate of 20 mV s^{-1} . The system was held at 2.00 V for 5 , 10 , or 15 min ; then, the reduction reverse scan to 0.00 V at 20 mV s^{-1} was performed. Before and after modification, 30 cyclic

voltammograms ranged from 0.00 to 1.60 V in $0.50\text{ mol L}^{-1}\text{ H}_2\text{SO}_4$ at a scan rate of 500 mV s^{-1} performed for current stabilization [22]. The current stabilization was evaluated by considering both capacitive and faradaic (gold oxides peak current) overlapping. The procedure was considered done when little to no difference in these values was perceived.

Electrochemical measurements

All measurements were carried out on an Autolab PGSTAT302N potentiostat equipped with a FRA2 impedance module (Metrohm, Netherlands) connected to a computer with the NOVA 2.0 software. pH measurements were taken using an 827 pH Lab pH meter (Metrohm, Switzerland), and a Fisatom 722 vortex shaking system (2800 rpm) was used to homogenize reagents better. A single-compartment three-electrode electrochemical cell containing 5.00 mL of supporting electrolyte was used for all electrochemical measurements. The working electrodes consisted of a bare bulk gold electrode (GE) and a nanoporous gold electrode (NPGE); the reference and auxiliary electrodes comprised Ag/AgCl, KCl sat, and platinum wire, respectively.

The electrochemical behavior of DCBQ was studied on both GE and NPGE in $0.10\text{ mol L}^{-1}\text{ BR}$ supporting electrolyte (pH 7.00) using cyclic voltammetry in a potential range of -0.30 – 0.80 V , at the scan rate of 20 mV s^{-1} . Afterward, the modified electrode was used to record cyclic voltammograms (CVs) in $0.50\text{ mol L}^{-1}\text{ H}_2\text{SO}_4$ from a lower potential of 0.00 V to a potential of 1.60 V , at a scan rate of 100 mV s^{-1} . Data recorded were used to obtain the electrochemical surface area (ECSA) of the electrodes, based on the following equation:

$$\text{ECSA} = \frac{Q}{\text{SSA}}$$

Q is the total charge of the reduction peak in the reverse scan, and SSA is the specific surface area of the crystal structure, assumed to be $390\text{ }\mu\text{C cm}^{-2}$ [23]. The total charge is obtained by dividing the integrated reduction peak area, determined by Nova software, with the measurement's scan rate (100 mV s^{-1}).

Electrochemical impedance spectroscopy (EIS) measurements were performed in $0.10\text{ mol L}^{-1}\text{ KCl}$ containing $5.00\text{ mmol L}^{-1}\text{ [Fe(CN)}_6\text{]}^{3-/4-}$ at an

applied potential of 272 mV versus Ag/AgCl. A frequency range between 100 kHz and 100 mHz at an amplitude of 10 mV was used. The Nyquist plots were represented by the intersection of the real (Z') and the imaginary ($-Z''$) coordinate axes, which results in a semicircle at the high-frequency region and a line at low frequencies. Based on the data from the plots, equivalent circuits were obtained, where R_s represents the uncompensated solution resistance, R_p denotes electron transfer resistance element, and CPE designates the constant phase element that defines the double-layer capacitance according to the Randles cell model.

The pH study was realized using BR supporting electrolyte in a pH range of 3.00–8.00 by the linear sweep voltammetry (LSV) technique at the scan rate of 100 mV s^{-1} (-0.20 to 0.70 V). Using the same technique, a study for scan rate was performed, varying its value from 1 to 400 mV s^{-1} . To evaluate the monolayer homogeneity and electrons number in the overall reaction process, the full width at half maximum (FWHM) was obtained according to the equation [24]:

$$\text{FWHM} = 3.53 \frac{RT}{nF} = \frac{90.6}{n}$$

F is $96.485 \text{ C mol}^{-1}$, n is the number of electrons transferred, T is temperature, and R is the ideal gas constant [24].

Cyclic voltammetry (CV), differential pulse voltammetry (DPV), square wave voltammetry (SWV), and linear sweep voltammetry (LSV) techniques were analyzed for sensible DCBQ determination. The one with a higher current signal was chosen, and all parameters of the proposed method were optimized. The calibration curves were then constructed by the successive addition of different volumes of the standard solution in the electrochemical cell. Figures of merit such as limit of detection (LOD), the limit of quantification (LOQ) were obtained using the following equations [25, 26]:

$$\text{LOD} = \frac{3S_b}{s}; \text{LOQ} = \frac{10S_b}{s}$$

S_b is the standard deviation value of ten measured blanks, and s is the calibration curve slope. Every measurement was realized at least in triplicate ($n = 3$), and, whenever necessary, the blank subtraction was made to understand better and visualize the peak current faradaic contribution.

A repeatability and reproducibility study was carried out to assess the accuracy of the proposed method in determining DCBQ; for this purpose, the analytical signal was obtained from a series of 10 consecutive voltammograms (repeatability) and 10 different electrodes (reproducibility) under previously optimized conditions. The relative standard deviations (RSD) of the tests were calculated according to the equation, as follows [25, 27]:

$$\% \text{RSD} = S \cdot \frac{100}{X}$$

where S is the value of the standard deviation and X is the average value between the measurements.

Recovery tests are related to the method's accuracy, as it reflects the amount of the analyte studied recovered in the process, concerning the actual value present in the sample [25, 27]. Levels of DCBQ (5 , 10 , and $15 \mu\text{mol L}^{-1}$) were chosen to fortify water samples, considering the linear range found in the analytical curve and the sensor aims applications in low concentration values. For this study, tap water (treated by chlorination) and deionized water were analyzed. The following equation was used to calculate the percent recovery, and its value should vary from $80,00$ to $110,00\%$ for good analytical acceptance [25, 27].

$$\% \text{Recovery} = \frac{(\text{obtained value} - \text{real value})}{\text{real values}} \times 100$$

Physical characterizations

All atomic force microscopy (AFM—Flex-AFM, Nanosurf, Switzerland) images were obtained in contrast phase mode on an active vibration isolation table (model TS-150, Table Stable LTD®) using a silicon Tap190G cantilever (resonant frequency 190 kHz , force constant 48 N/m , Budget Sensors) in setpoint of 50% . X-ray photoelectron spectroscopy (XPS) analyses were performed with an ESCA + spectrometer system equipped with an EA 125 hemispherical analyzer and XM 1000 monochromated X-ray source (Scienta Omicron, Uppsala, Sweden) in $\text{Al K}\alpha$ radiation (1486.7 eV). The calibration used the $\text{C } 1s$ peak ($\text{BE} = 284.8 \text{ eV}$). CasaXPS processing software version 2.3.15 (Casa Software Ltd., Teignmouth, UK) was used for the data analyses. Field-strength scanning electron microscopy (FEG-SEM, also named SEM in the entire

manuscript) images were obtained using JEOL® JSM-IT300 (JEOL, Tokyo, Japan), operating at 5 kV.

Results and discussion

Electrochemical effect of time on the anodization

An anodization–reduction process is a unique approach for GEs 3D surface modification. Usually, the method starts with anodization up to a particular potential, holds for a while, and promotes the reverse scan. However, one may notice that such a procedure has to be carefully investigated once it can cause detrimental effects on the electrode due to prolonged exposition of the applied potential, diminishing its usage considerably. Thus, three different times were chosen—5, 10, and 15 min—to evaluate the effect of anodizing time on gold's electrochemical behavior in a $0.50 \text{ mol L}^{-1} \text{ H}_2\text{SO}_4$ solution, as depicted in Fig. S1. The prominent oxidation waves at 1.19 V and 1.40 V indicate Au's preferential orientation (100) and Au (111) crystal planes [28]. Also, the augmented current response observed resulted from increasing the electroactive area due to the potential exposure time. By the results available in Fig S1 regarding the current response, the 15-min modification seemed to be the best choice and was used further in the manuscript.

ECSA analyses were performed once it is an essential factor to assess the materials' reactivity in conformity with the current previous results. The process resulted in the surface areas of 0.14, 0.42, and 0.95 , and 2.22 cm^2 for the unmodified and 5-, 10-, and 15-min modified GEs, respectively. The GE modification with 15 min holding at 2.00 V (according to the experimental section) presents the higher electrochemical surface area, which is interesting for our sensing applications proposes. Nevertheless, the surface modification needs to be analyzed to evaluate the damage degree of the surface, aiming for a reproducible and reusable electrode.

State-of-the-art electrochemical approach to fabricate NPGs

Most literature on the subject leans toward analyzing the role of the anodization–reduction process by SEM. Figure 1a) shows the unmodified electrode as it

is; it is noticeable the absence of nanoporous on GE's before the electrochemical process, with typical random surface roughness and scratches due to the mechanical polishing [29]. Following the electrode's

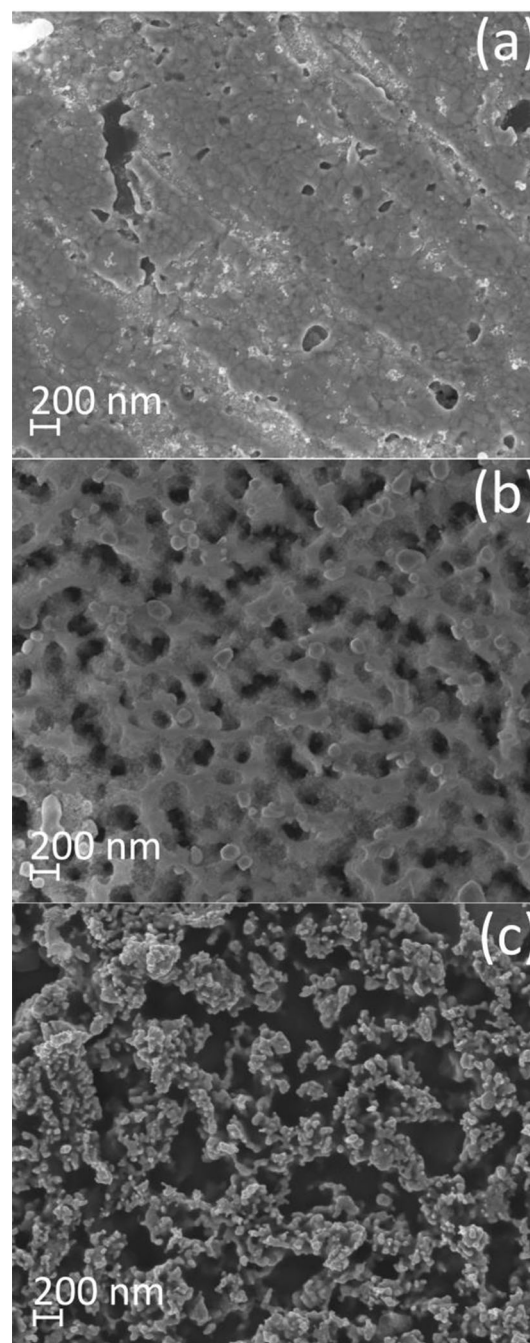


Figure 1 SEM images of the GE at three different stages: **a** unmodified gold electrode surface; **b** gold surface after anodization at 2.00 V, held for 15 min (forward scan); and **c** gold surface after electrochemical reduction to 0.00 V (reverse scan). The surface modification was carried out in a $0.50 \text{ mol L}^{-1} \text{ H}_2\text{SO}_4$ solution at a scan rate of 20 mV s^{-1} .

electrochemical modification, Fig. 1b) demonstrates that the anodization process at 2.00 V was efficient for the GE surface modification (15 min), i.e., a distinguished three-dimensional nanoporous network structure was observed. According to Cherevko et al., the electrochemical oxidation and the dissolution of Au occur at similar potentials, forming simultaneously several forms of oxides, hydroxides, or hydrous oxides on the gold surface, while the formation of Au^{3+} ions causes diffusion from the vicinity of the electrode [30]. Although Au^{3+} species are stable in acidic solutions at appropriate positive potentials, the formation of the gold oxides causes passivation to the system, not allowing a substantial dissolution of gold, which occurs due to a transient gold dissolution step [30, 31]. Such a process may explain the nanoporous structure formation observed.

Figure 3c) shows the SEM image acquired after the electrochemical reduction reverse scan to 0.00 V. It can be seen an even more porous structure than in Fig. 1b). Although the exact process is not straightforward, some observations are possible based on the Cherevko et al. studies: (1) The gold re-deposition is negligible in the time scale of the experiments due to kinetics as the ions are not located in the double-layer region of the electrode; (2) the negative-going sweep causes the reduction of the oxides formed before; (3) such process seems to have a similar transient dissolution of the gold mechanism of the anodization; (4) the dissolution process is higher in the reduction process [30]. Thus, the massive increase in the electrode's porosity can be explained and corroborates that 15 min of anodization was the best choice once higher exposition times would be detrimental for the electrode's surface. Also, the results suggested an augmentation of the roughness of the electrode surface.

However, by SEM images, we were not able to evaluate the surface modification fully. For improved analyses, the AFM technique was employed. Figure 2 shows topography images of the electrode surface in the three stages. The AFM images are related to mechanical and electrochemical processes. In Fig. 2a, b), it is noticed that the electrode before anodization presents a smoother surface, as expected, although it is possible to verify scratches on the surface caused by the polishing process. After the electrochemical corrosion, a considerable increase in the surface's roughness was achieved (Fig. 2c, d)), slightly increasing after the reduction stage (Fig. 2e, f)).

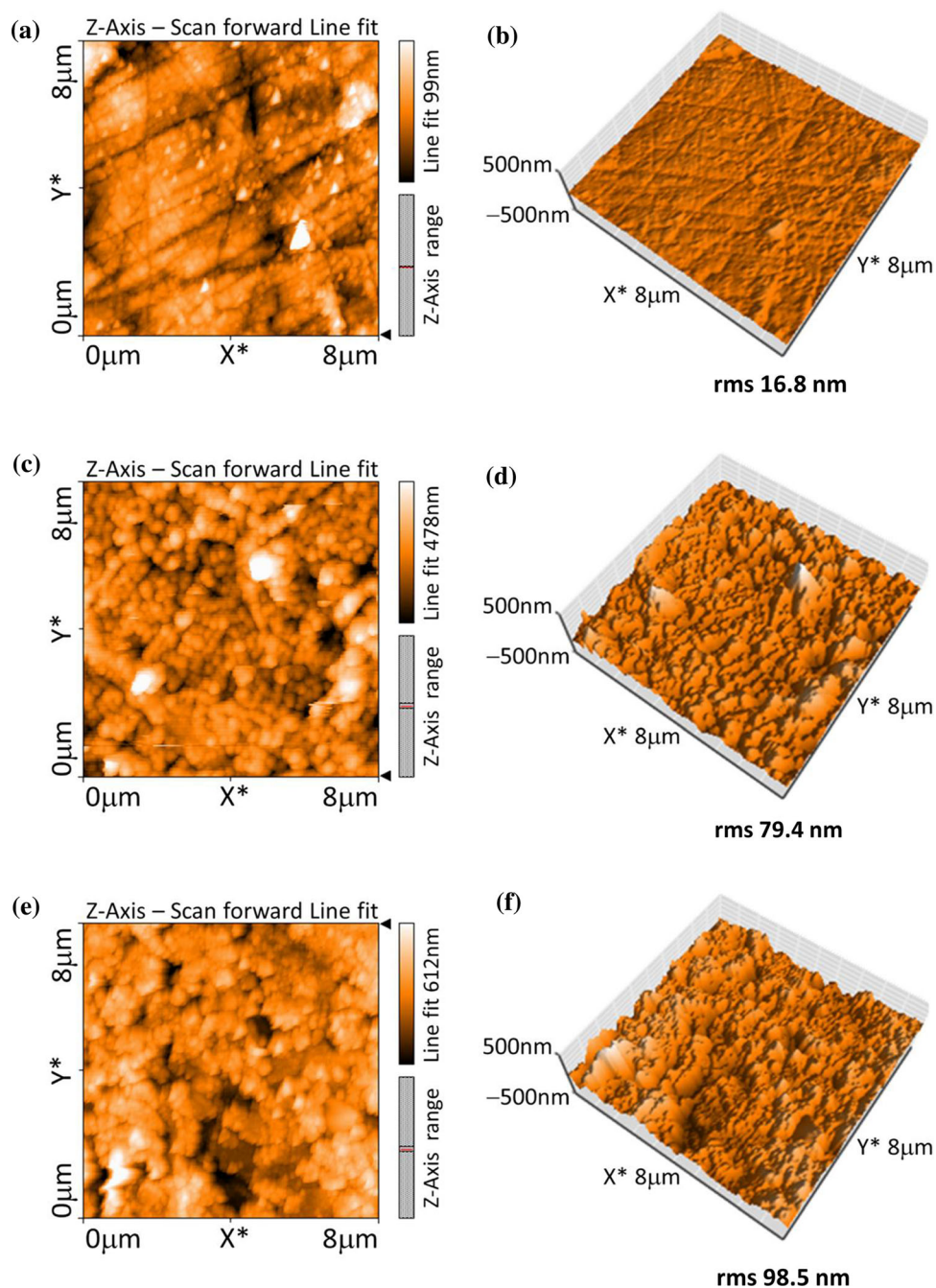
As the roughness of surfaces can be studied by domain parameters, such as roughness average and root mean square (rms) roughness, these parameters can be used to compare changes on the substrate surfaces [32]. Once the latter is considered more sensitive for deviations from the mean line/plane, we decided to use it as the comparison parameter. Thus, the rms values presented by the GE are 16.8, 79.4, and 98.5 nm to the polished, after anodization, and after reduction processes, respectively. The increase in the rms observed by AFM analyses indicates the enlargement of the surface area of the GE after the electrochemical anodization and reduction process; the higher the rms factor, the higher the surface area of the substrate. It is worth noting that the AFM data agree with the SEM data, which shows the rise in porous in the GEs surface after electrochemical treatment. The surface's roughness significantly increased compared to the unmodified GE, indicating successful electrode surface modification.

One can notice that based on SEM and AFM analyses, such three-stage surface modifications of the GE not only promote an increase in the surface area but also are responsible for the formation of an adlayer of gold hydroxide/oxide. Thus, the nature of the adsorption of species is different from the unmodified GE, which can be interesting for sensing applications, as discussed further [33].

Thus, to investigate GE's surface composition and chemical states' changes after the anodization–reduction process, XPS spectra were collected from the sample at the three stages. The wide-scan survey spectra (low-energy resolution) for the three stages present only Au, O, and C, attesting to the high purity of the chosen electrode; consequently, the same was observed for the other stages (Fig. 3a). However, the narrow-scan high-resolution spectra show different gold chemical states. One can notice that two pairs of peaks are observable in all the spectra (Fig. 3b, c) due to $\text{Au}_{4f7/2}$ and $\text{Au}_{4f5/2}$ spin-orbit coupling. Figure 3b) shows peaks located at 84.02 and 87.72, attributed to Au^0 species, while the peaks located at 86.09 and 879.85 eV are related to Au^{3+} species. Similar peaks are observed to the electrode at different stages, with slight shifts.

Although the same chemical species are present in the three stages, the relative peak areas from 1 to 2 stages are significantly altered. (Stage 1 and 2 are before and after electrochemical anodization, respectively.) On this basis, the atomic percentages

Figure 2 AFM images of the electrode at three different stages: **a** and **b** before anodization; **c** and **d** after anodization at 2.00 V; and **e** and **f** after reduction to 0.00 V.

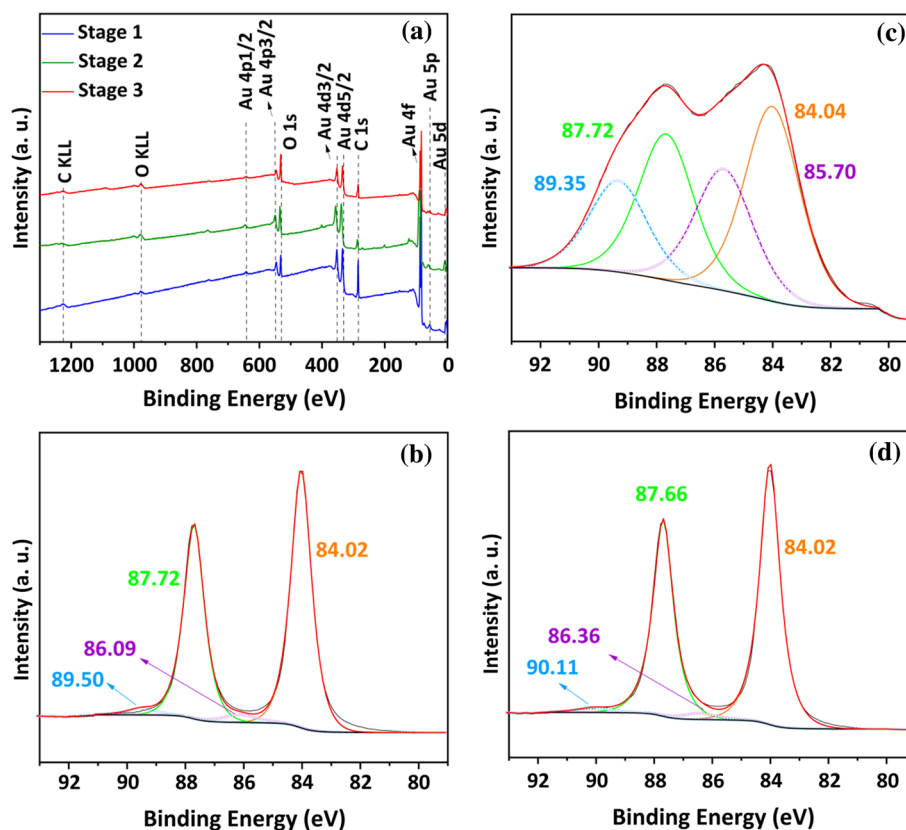


were estimated as 95.08% for Au^0 and 4.92% for Au^{3+} for the electrode at stage 1. On the other hand, the electrode at stage 2 presented 60.57% and 39.43% for Au^0 and Au^{3+} , respectively. The XPS technique attested quantitatively what SEM and AFM showed before: the surface's oxidation after the anodization. Nevertheless, after the reduction reverse scan (stage 3), the phenomenon observed is more impressive: 96.12% and 3.88% for Au^0 and Au^{3+} , respectively (Table S1). This result corroborates the data discussed

before: Although there is Au^{3+} dissolution to the bulk solution, the reverse scan can reduce most oxidized species on the electrode surface. The process virtually leaves the electrode to the same condition as before the anodization–reduction procedure, however, with the surface modified. Such information is highly essential to verify the electrode working conditions, as presented next.

After all the physicochemical characterizations performed herein, we could attest to its 3D

Figure 3 a XPS low-energy resolution spectra of the electrode at the three different stages. The electrode's high-resolution spectra at the same stages: b before anodization; c after anodization at 2.00 V; and d after reduction to 0.00 V.



nanoporous surface nature. Thus, the modified electrode can be correctly designed as a nanoporous gold electrode (NPGE) from now on.

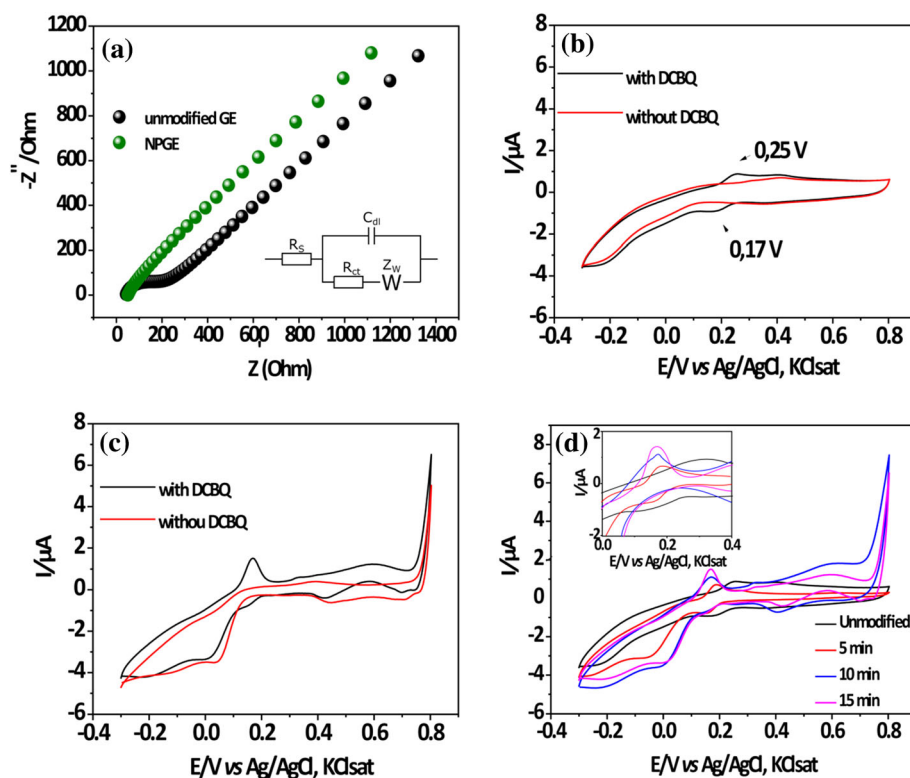
Impedance measurement and effect of the modification on the DCBQ detection

Based on the data obtained, it was noteworthy that the 15-min modification process presented the best electrochemical area and current response without intense damage on the electrode surface. An additional electrochemical characterization used to assess the performance and properties of the NPGE is EIS (Fig. 4a). The Nyquist plots obtained from the unmodified GE and NPGE enabled us to calculate solution resistances of 161.00 Ω and 3.90 Ω (see Randles equivalent circuit model in Fig. S2), respectively. As expected, such data strongly indicate the dissimilar structure and electrochemical performance after the electrode modification, corroborating the physicochemical characterizations. However, the unmodified GE presented higher charge transfer resistance than the NPGE, which is unsuitable for sensing issues. Thus, the surface area augmentation obtained

in the anodization–reduction prompted a more conductive electrode.

Such results are highly related to the electrochemical response of the DCBQ substrate on the electrode (Fig. 4b, c). Also, such data allow us to evaluate the properties of the prepared electrode, using it to observe any electrocatalytic performance [34]. The effect of the modification treatment on the obtained CV curves without the substrate was intensifying in the capacity current and faradaic processes [33]. The same was observed with the substrate (recorded in a potential range of -0.30 to 0.80 V, 20 mV s $^{-1}$, 0.10 mol L $^{-1}$ Britton–Robinson buffer ionic strength, pH = 7.00), validating the larger surface area for the modified material. Besides the intensification, the modification also caused oxidation (0.25 V/ 0.17 V) and reduction (0.17 V/ 0.15 V) potential swifts for the unmodified GE and NPGE, respectively, indicating an electrocatalytic behavior due to the surface modification carried out. Also, the modification drove a remarkable increase in the anodic (232.56%) faradaic current peak contribution. Moreover, the following measures will be done in the anodic region due to this great augment in the anodic current peak

Figure 4 **a** Nyquist plots for the unmodified GE and NPGE. **b** CV for the unmodified GE with and without the substrate. **c** CV for the NPGE with and without the substrate. **d** CV of the different modification times of the GE. Data were recorded in 0.10 mol L^{-1} Britton–Robinson buffer ionic strength, $\text{pH} = 7.00$, scan rate = 20 mV s^{-1} , $[\text{DCBQ}] = 99.00 \text{ } \mu\text{mol L}^{-1}$.



compared to the unmodified electrode. The same trend of potential shift and intensification was obtained with the modification time (Fig. 4d), following the physicochemical characterizations and previous electrochemical analyses. However, the increase in the electrochemical surface area does not imply the same response in the faradaic current due to kinetics issues [35]. Therefore, the differences in electrocatalytic activity cannot be related to differences in the surface area. As a result, these results indicate that the nature of the surface modification strongly affected the detection and electrocatalytic sensitivity toward DCBQ.

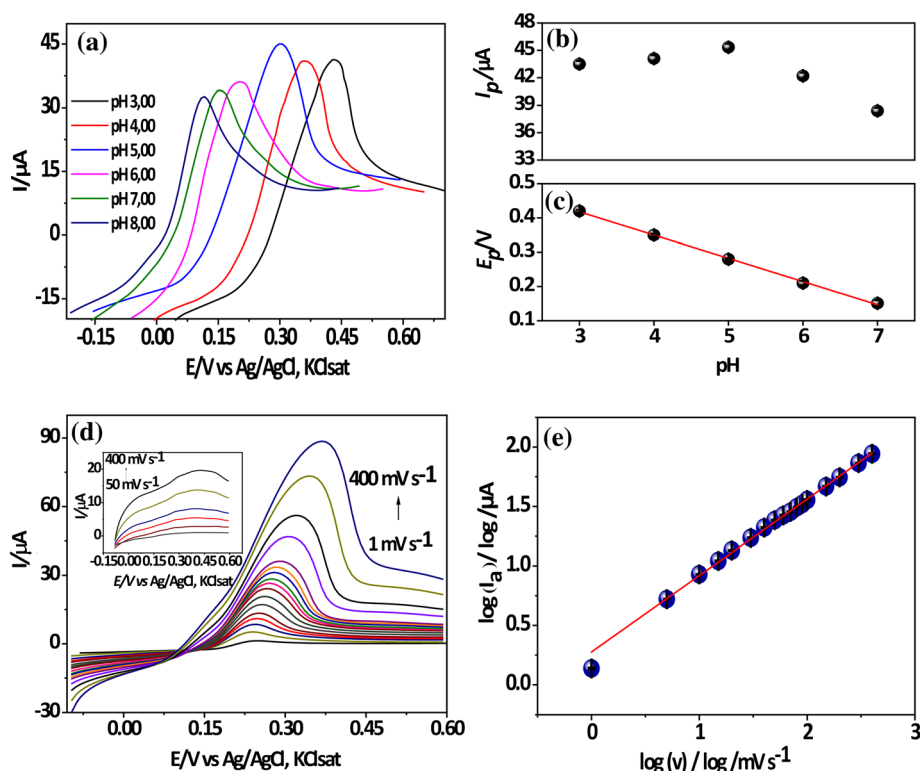
Effect of pH and scan rate on the DCBQ voltammetric response

A detailed pH dependence study to evaluate the optimum charge transfer rate for the sensor was performed. At first glance, we observed that the DCBQ's electrocatalytic degradation process was higher at alkaline media, which was expected once the compound is prone to hydrolysis at such environments, resulting in a hydroxyl-substituted compound [36]. Thus, the pH effect was evaluated in a limited pH range ($\text{pH} = 3.00, 4.00, 5.00, 6.00, 7.00,$

and 8.00) at a scan rate of 20 mV s^{-1} (Fig. 5a). A strong pH effect is evident on the voltammograms, with a quasi-linear increase in the I_p with pH increasing up to 5.00 , with an I_p reduction over this pH (due to stability issues of the DCBQ) [37]. Such a trend indicated that protons participate in the electrode's process and that the NPGE is a suitable platform to prepared sensors for DCBQ detection. From this plot, it was also possible to obtain an FWHM of 0.052 ± 0.004 , allowing for a number of electrons of 1.70 , which follows the literature redox mechanism of 2-electron transfer with 2 protons [38]. From Fig. 5b, one can notice that the plot of E_p versus pH in the pH range considered provided one linear relationship of $E_p = 0.62 - 0.06 (\text{pH})$; $r = -0.9995$. The obtained slope suggests an equal number of protons and electrons in DCBQ oxidation according to the theoretical 0.0592 V/pH . Figure 5c presents a plot of I_p versus pH with an enhanced peak in pH 5; thus, this pH was maintained throughout studies [39].

The LSV technique evaluated the effect of the scan rate. The potentials of DCBQ shifted to positive values with the scan rate increase (Fig. 5d) with peak area increase. The equation attained from the plot I_p versus $v^{1/2}$ presented a linear correlation with an $r = 0.9932$ that suggests a process ruled by diffusion.

Figure 5 **a** Linear sweep voltammograms recorded with NPGE in BR buffer 0.10 mol L⁻¹, **b** peak current versus pH, and **c** peak potential versus pH (presence of DCBQ 5.00 mmol L⁻¹, pH range 3.00–8.00). **d** Linear sweep voltammograms recorded with NPGE. **e** Dependence of the log (anodic current) versus log (scan rate) (presence of DCBQ 2.00 mmol L⁻¹, scan rate ranging from 1 to 400 mV s⁻¹ and the inset of Figure 5d–400 mV s⁻¹ of blank measures).



Besides, the plot of $\log I_p$ versus $\log v$ gave a slope of 0.64, near the theoretical 0.50, suggesting a diffusion-controlled process [40].

Sensing performance optimization

We were able to qualitative/quantitatively evaluate the NPGE surface and made some pertinent considerations upon applying such an electrode for DCBQ detection. Also, we proved that the conditions and time were the ideal ones for achieving a substantial change on the GE surface. However, the utilization of gold is an essential issue for electrocatalytic sensing, taking advanced on the surface nanostructuring of our system. Thus, in the next step, we decided to investigate the performance of the NPGE on the electrocatalytic detection of 2,6-dichloro-1,4-benzoquinone. Four parameters were optimized—electrolyte composition, electrolyte concentration, voltammetric techniques for DCBQ sensing, and after the best voltammetric process was chosen, its optimization. The optimization of these parameters aims to develop a sensor with higher sensitivity in the determination of DCBQ.

Influence of different electrolyte buffers on the electrochemical response of DCBQ

The electrolyte buffers—acetate, Britton–Robinson, citrate, and phosphate—were assessed to be used herein to fabricate a sensor with an optimized active electrode. By respecting the previously obtained pH = 5.00, such electrolytes were chosen due to their buffering capacity. The experiments were performed using the same concentration of buffer and substrate of 0.10 mol L⁻¹ and 49.75 $\mu\text{mol L}^{-1}$, respectively. It was found that an intensification in the current was achieved by using citrate buffer with the square wave voltammetry technique (Fig S3a). The current peak was obtained among 0.20 V e 0.35 V, with lower deviations in the data (Fig S3b). Such a buffer was chosen for the following experiments.

Influence of the concentration of citrate buffer on the electrochemical response of DCBQ

The effect of the citrate concentration on the electrochemical response of DCBQ was studied by employing the following concentrations: 0.025, 0.050, 0.10, 0.25, and 0.50 mol L⁻¹. Figure S3c shows the

voltammograms for the different concentrations of the solutions, and the optimum condition was defined through the current difference among the diverse concentrations. (Figure S3d presents the deviations in the data.) Almost a fourfold improvement in the DCBQ response was observed, from 0.50 to 0.10 and 0.025 mol L⁻¹. The chosen condition was 0.10 mol L⁻¹.

Voltammetry technique choice on the electrochemical response of DCBQ

Although the previous optimizations were performed using square-wave voltammetry, it cannot be the best method for the electrochemical response of DCBQ. Thus, SWV, CV, and VPD were carried out to compare which technique is the most suitable for DCBQ detection. Comparatively, SWV was the most sensitive technique, with less background charging current (non-faradaic processes), while CV was the least sensitive. Also, the SWV method showed the most prominent peak current for the oxidation of the substrate. The peak current shift observed for the SWV (0.27 V) when compared to CV (0.26 V) and VPD (0.23 V) is due to the forming characteristics of a capacitor and the internal resistance of the source of voltage related to each technique [41]. Based on the findings, the SWV method was chosen for the detection procedures.

Optimization of the SWV parameters

SWV parameters were optimized to enhance the electroanalytical current signals of the DCBQ detection, aiming to affect the height and resolution of the peak. The step potential (E_{step}) was recorded in a potential window from 1 to 10 mV exposed to 0.20 mmol L⁻¹ DCBQ (Fig. S4a). One can notice that a peak current increase was observed along with the step size rise, which can be better seen in Fig. S4b. However, the peaks' resolution suffered a decline with the E_{step} augmentation, which is not interesting for our proposals. Thus, 10 mV was selected for the E_{step} , demanding further optimizations based on the signal intensity.

The pulse amplitude was studied from 1 to 100 mV (Fig. S4c, d). As expected, the peak current increases at the variation of pulse amplitude. However, the peak resolution was lost over 80 mV, without a gain in the peak current, being such pulse amplitude

chosen for the successive experiments. The frequency is another parameter that affects the peak current in SWV, being studied in a range of 20–60 Hz. According to Fig. S4e, f, 25 Hz was selected as the frequency once it offers the highest sensitivity, with higher signal intensity. Under these parameters, the voltammetric measurements were obtained in just 2.4 s, which was used for the subsequent analytical applications.

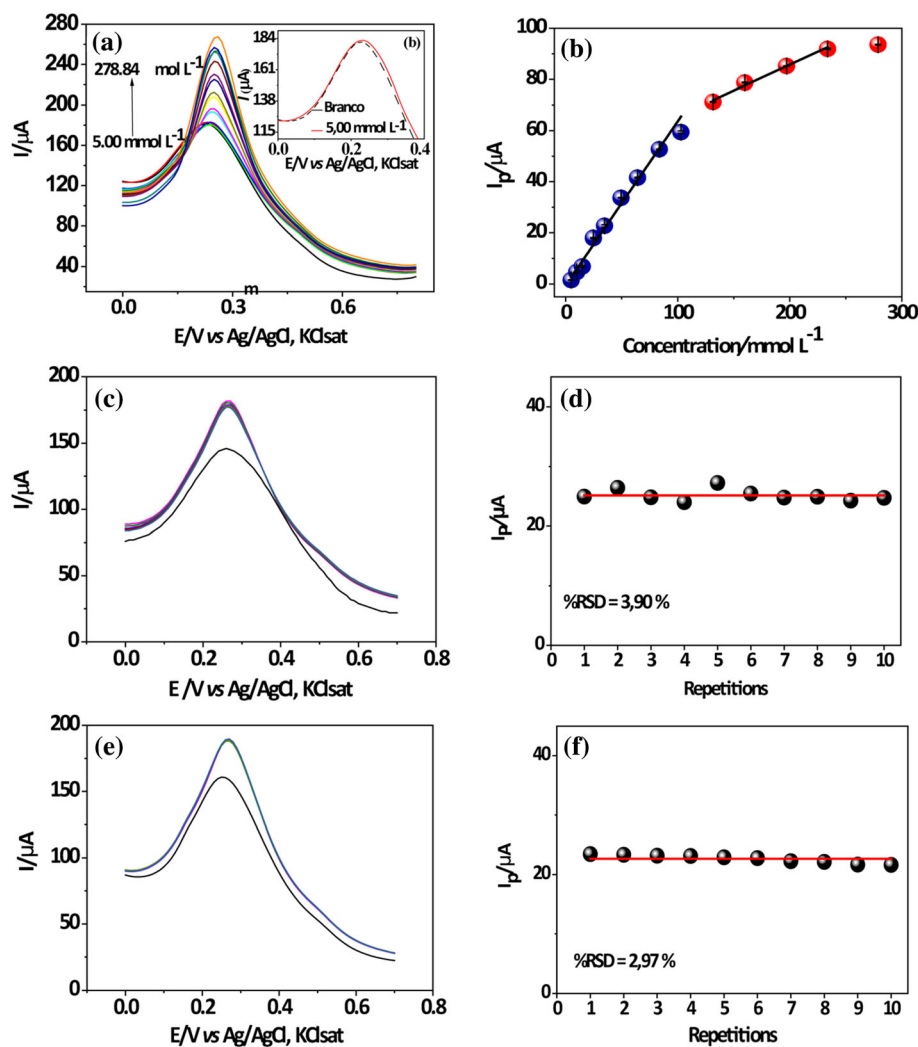
Analytical performance

Once the optimizations were performed, the analytical performance of the NPGE was tested. The calibration curve was performed for DCBQ concentrations from 5.00 to 278.84 $\mu\text{mol L}^{-1}$ at pH = 5.00 and 0.10 mol L⁻¹ citrate buffer (Fig. 6a). All the experiments were performed in triplicate ($n = 3$), and it was handled by subtracting the blank sample to permit only faraday currents. The calibration curve presented two linear ranges (Fig. 6b), which fit the following equations: $y = 0.64 \times - 0.53$ ($r = 0.9973$) and $y = 0.20 \times + 45.29$ ($r = 0.9955$). Such phenomenon is related to the 3D nanostructuring of the electrode performed, which promoted the formation of a complex surface with different equilibrium dissociation constants [42]. The detection limit, quantification limit, and sensibility were 0.77, 2.56, and 0.64 $\mu\text{A } \mu\text{mol L}^{-1}$, respectively. Although the literature may present lower quantification and detection limits [43–45], our system is fast, low-cost, and easy to handle. A pre-concentration step can handle lower concentrations of the substrate. [46]

Repeatability and reproducibility: material analyses explanation of the electrochemical data

Repeatability and reproducibility are two crucial parameters to evaluate the sensor performance. These parameters are essential to assess the operational period of the sensor under working environment conditions [47]. The NPGE presented an R.S.D of 3.90% for ten repetitive measurements using the same electrode, which underwent 10 modifications before the analyses (Fig. 6c, d). Also, it offered a remarkable reproducibility, with R.S.D of 2.97% for ten repetitive measurements using the same electrode, however, with the same modification (Fig. 6e, f).

Figure 6 **a** SWV, **b** blank and **c** peak currents recorded for the NPGE. DCBQ concentration: 5.00 to 278.84 $\mu\text{mol L}^{-1}$. **d** SWV and **e** peak current for reproducibility tests. **f** SWV and **g** peak current for repeatability tests. Conditions for (d–g): DCBQ concentration: 49.75 $\mu\text{mol L}^{-1}$. The experimental conditions were: 0.10 mol L^{-1} citrate buffer, scan rate = 20 mV s^{-1} , frequency = 25 Hz, $E_{\text{step}} = 10 \text{ mV}$, $E_{\text{amp}} = 80 \text{ mV}$.



The same characterizations carried out with the as-modified electrode were performed after the ten repetitive measurements (for the reproducibility tests) to understand better such results based on materials' analyses. In Fig. 7a, the SEM image shows remarkable modifications on the electrode's surface compared to Fig. 1c. The same effect is observed with AFM analysis after repeatability tests (Fig. 7b, c). Although the rms obtained was 98.6 nm, and its value is near that estimated before DCBQ detection (98.5 nm), there are evident changes in the topography of the NPGE. It is noticed that the presence of large agglomerates and the interaction of AFM's tip with the surface is impaired, probably due to the adsorption of by-products on the NPGE surface after DCBQ oxidation.

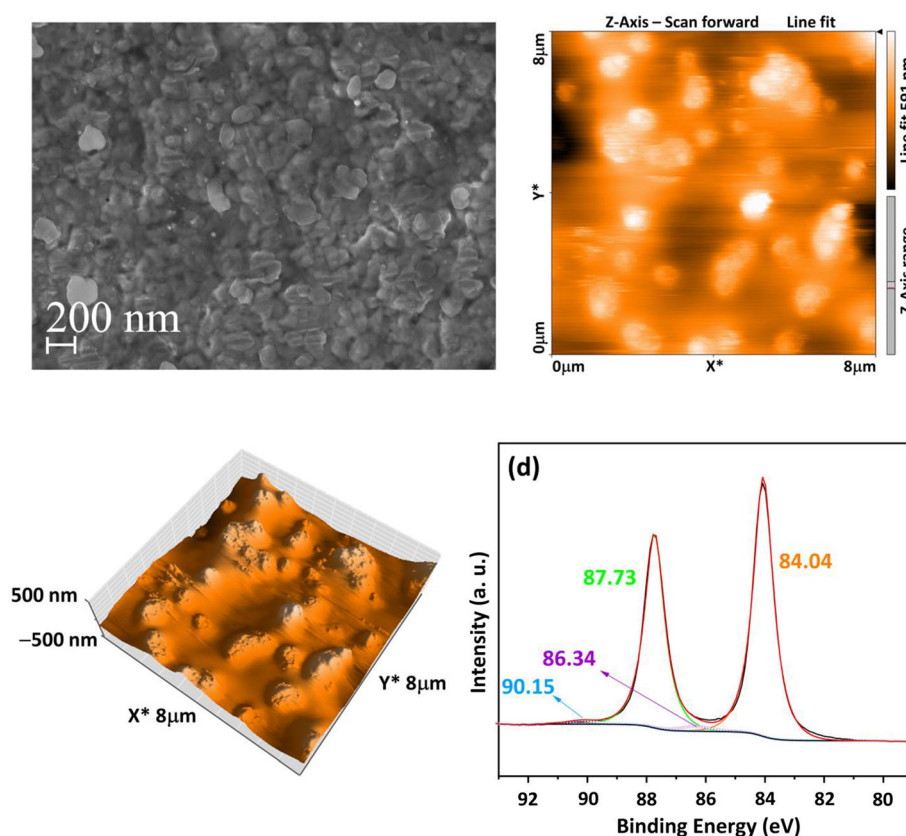
Further, the analysis with XPS, which was performed after the measurements, shows the same

chemical states for the as-modified electrode, i.e., the two pairs of peaks of $\text{Au}_{4f7/2}$ (Au^0 species: 84.04 and 87.73 eV) and $\text{Au}_{4f5/2}$ (Au^{3+} species: 86.34 and 90.15 eV) are present with slight shifts. The atomic percentages were estimated as 91.11% for Au^0 and 2.89% for Au^{3+} . Consequently, the XPS analysis shows the preservation of the electrode surface regarding the chemical states of the gold surface. Thus, although changes were observed, the analytical electrode's response is the same.

Real sample analysis: tap water and recovery method

One of the major challenges in electrocatalytic detection is to remove the interfering responses generated by some endogenous species. Therefore, deionized water was also investigated with tap water

Figure 7 a SEM image, b, c AFM images of the electrode, and c XPS low-energy resolution spectra of the NPGE after ten repetitive measurements.



(Figs. S3 and S4). Thus, we decided to use the recovery method for the analyses performed herein, which consists of spiking a known amount of an analyte solution [48]. For that, three different DCBQ concentrations were used—5.00, 10.00 and 15.00 $\mu\text{mol L}^{-1}$ —according to the linear range of the calibration curve. According to Table 1, there was no significant matrix effect as remarkable accuracies with recovery percentages between 98.80 and 107.30% for the deionized water were obtained, while recovery percentages among 101.10 and 107.60% were achieved for the tap water. Such results are essential for our plans once the sample preparation is not an issue before the analyzing using our sensor. Based on such satisfactory data, we can affirm the

effectiveness of the developed system for DCBQ detection on real samples.

Conclusions

We performed a systematic experimental investigation on the electrocatalytic sensing activities of DCBQ on an NPGE as a function of its electrochemical surface modification. We were able to attest that the detection, before optimization, displayed a time of modification-dependent behavior, following an increased activity with exposition to 2.00 V anodization process time. SEM, AFM, and XPS analyses explained the higher catalytic activity for the 15-min

Table 1 Recovery tests performed with deionized and tap water

Matrix	DCBQ ($\mu\text{mol L}^{-1}$)	Concentration ($\mu\text{mol L}^{-1}$)	Recovery (%)
Deionized water	5.00	4.94 ± 0.06	98.80
Deionized water	10.00	10.87 ± 0.63	108.70
Deionized water	15.00	16.09 ± 0.60	107.27
Tap water	5.00	5.30 ± 0.34	107.60
Tap water	10.00	10.70 ± 0.70	107.30
Tap water	15.00	15.00 ± 0.95	101.10

modified electrode as the modification process was efficient; also, we were able to show that the routine was not an area issue. To the best of our knowledge, this is the first time that physical–chemical characterizations have explained the performance of an NPGE. Also, we were able to evaluate the electrochemical reproducibility using the same materials characterization methods, showing that the system presented some damage but maintained its analytical response. After the optimizations, the NPGE gave efficiency for the real sample tap water analyses, showing low/no matrix effects as remarkable accuracies with recovery percentages were achieved. LOD and LOQ, as well as the system sensibility, showed excellent results for the sensing probe. The electroanalytical detection of DCBQ in treated water samples by an NPGE is yet to be reported in the literature, as this is the first work that shows such results. We highly believe that our result will provide new opportunities to evaluate and develop new NPGEs electrocatalytic sensors with enhanced properties. The applications of the NPGE presented a potential for more uses, with a great approach in analytical performances.

Acknowledgements

This work was supported by: National Council for Scientific and Technological Development—CNPq (Grant No. 205220/2018-5; 465389/2014-7); Foundation for the Support of Research, Scientific and Technological Development of Maranhão—FAPEMA (Grant No. 01372/17-UNIVERSAL); Coordination of Superior Level Staff Improvement—CAPES (Grant No. 88887.472618/2019-00-PROCAD-AM, 88882.445688/2019-01); H.-B. Kraatz is grateful for financial support from Canada's Natural Sciences and Engineering Research Council (RGPIN-2016-06122) and from the University of Toronto Scarborough.

Declarations

Conflict of interest The authors declared that they have no conflicts of interest in this work.

Supplementary Information: The online version contains supplementary material available at <https://doi.org/10.1007/s10853-021-06616-4>.

References

- [1] Nasrollahzadeh M, Sajjadi M, Soufi GJ et al (2020) Nanomaterials and nanotechnology-associated innovations against viral infections with a focus on coronaviruses. *Nanomaterials*. <https://doi.org/10.3390/nano10061072>
- [2] Srivastava M, Srivastava N, Mishra PK, Malhotra BD (2021) Prospects of nanomaterials-enabled biosensors for COVID-19 detection. *Sci Total Environ* 754:142363. <https://doi.org/10.1016/j.scitotenv.2020.142363>
- [3] Noah NM (2020) Design and synthesis of nanostructured materials for sensor applications. *J Nanomater*. <https://doi.org/10.1155/2020/8855321>
- [4] Gualteros JAD, Garcia MAS, da Silva AGM et al (2018) Synthesis of highly dispersed gold nanoparticles on Al₂O₃, SiO₂, and TiO₂ for the solvent-free oxidation of benzyl alcohol under low metal loadings. *J Mater Sci*. <https://doi.org/10.1007/s10853-018-2827-x>
- [5] Patrícia R, Castro K, Aurélio S, Garcia M, de Abreu CW et al (2018) Aerobic oxidation of benzyl alcohol on a strontium-based gold material: remarkable intrinsic basicity and reusable catalyst. *Catalysts* 8:83. <https://doi.org/10.3390/cata18020083>
- [6] De Abreu WC, Garcia MAS, Nicolodi S et al (2018) Magnesium surface enrichment of CoFe₂O₄ magnetic nanoparticles immobilized with gold: reusable catalysts for green oxidation of benzyl alcohol. *RSC Adv* 8:3903–3909. <https://doi.org/10.1039/c7ra13590d>
- [7] Gonçalves JM, Kumar A, da Silva MI et al (2021) Nanoporous gold-based materials for electrochemical energy storage and conversion. *Energy Technol* 9:1–40. <https://doi.org/10.1002/ente.202000927>
- [8] Sukeri A, Arjunan A, Bertotti M (2020) New strategy to fabricate a polydopamine functionalized self-supported nanoporous gold film electrode for electrochemical sensing applications. *Electrochem Commun* 110:106622. <https://doi.org/10.1016/j.elecom.2019.106622>
- [9] Rossi LM, Fiorio JL, Garcia MAS, Ferraz CP (2018) Role and fate of capping ligands in colloiddally prepared metal nanoparticle catalysts. *Dalt Trans*. <https://doi.org/10.1039/C7DT04728B>
- [10] Qi X, Balankura T, Zhou Y, Fichthorn KA (2015) How structure-directing agents control nanocrystal shape: polyvinylpyrrolidone-mediated growth of Ag nanocubes. *Nano Lett* 15:7711–7717. <https://doi.org/10.1021/acs.nanolett.5b04204>
- [11] Guo T, Yao MS, Lin YH, Nan CW (2015) A comprehensive review on synthesis methods for transition-metal oxide nanostructures. *CrystEngComm* 17:3551–3585. <https://doi.org/10.1039/c5ce00034c>

- [12] Zhao H, Lei Y (2020) 3D Nanostructures for the next generation of high-performance nanodevices for electrochemical energy conversion and storage. *Adv Energy Mater* 10:1–8. <https://doi.org/10.1002/aenm.202001460>
- [13] Stine KJ (2019) Nanoporous gold and other related materials. *Nanomaterials* 9:13–15. <https://doi.org/10.3390/nano9081080>
- [14] Munonde TS, Nomngongo PN (2021) Nanocomposites for electrochemical sensors and their applications on the detection of trace metals in environmental water samples. *Sensors (Switzerland)* 21:1–27. <https://doi.org/10.3390/s21010131>
- [15] Sáenz HSC, Hernández-Saravia LP, Selva JSG et al (2018) Electrochemical dopamine sensor using a nanoporous gold microelectrode: a proof-of-concept study for the detection of dopamine release by scanning electrochemical microscopy. *Microchim Acta*. <https://doi.org/10.1007/s00604-018-2898-z>
- [16] Sukeri A, Lima AS, Bertotti M (2017) Development of non-enzymatic and highly selective hydrogen peroxide sensor based on nanoporous gold prepared by a simple unusual electrochemical approach. *Microchem J* 133:149–154. <https://doi.org/10.1016/j.microc.2017.03.023>
- [17] Shi L, Rong X, Wang Y et al (2018) High-performance and versatile electrochemical aptasensor based on self-supported nanoporous gold microelectrode and enzyme-induced signal amplification. *Biosens Bioelectron* 102:41–48. <https://doi.org/10.1016/j.bios.2017.11.012>
- [18] Liu Z, Nemecek-Bakk A, Khaper N, Chen A (2017) Sensitive electrochemical detection of nitric oxide release from cardiac and cancer cells via a hierarchical nanoporous gold microelectrode. *Anal Chem* 89:8036–8043. <https://doi.org/10.1021/acs.analchem.7b01430>
- [19] Francis NJ, Knospe CR (2019) Fabrication and characterization of nanoporous gold electrodes for sensor applications. *Adv Eng Mater* 21:1–13. <https://doi.org/10.1002/adem.201800857>
- [20] van der Zalm J, Chen S, Huang W, Chen A (2020) Review: recent advances in the development of nanoporous Au for sensing applications. *J Electrochem Soc* 167:037532. <https://doi.org/10.1149/1945-7111/ab64c0>
- [21] Sukeri A, Saravia LPH, Bertotti M (2015) A facile electrochemical approach to fabricate a nanoporous gold film electrode and its electrocatalytic activity towards dissolved oxygen reduction. *Phys Chem Chem Phys* 17:28510–28514. <https://doi.org/10.1039/c5cp05220c>
- [22] Silva LSR, López-Suárez FE, Perez-Cadenas M et al (2016) Synthesis and characterization of highly active Pb_x@Pty/C core-shell nanoparticles toward glycerol electrooxidation. *Appl Catal B Environ* 198:38–48. <https://doi.org/10.1016/j.apcatb.2016.04.046>
- [23] Lukaszewski M, Soszko M, Czerwiński A (2016) Electrochemical methods of real surface area determination of noble metal electrodes: an overview. *Int J Electrochem Sci* 11:4442–4469. <https://doi.org/10.20964/2016.06.71>
- [24] Eckermann AL, Feld DJ, Shaw JA, Meade TJ (2010) Electrochemistry of redox-active self-assembled monolayers. *Coord Chem Rev* 254:1769–1802. <https://doi.org/10.1016/j.ccr.2009.12.023>
- [25] Marson BM, Concentino V, Junkert AM et al (2020) Validation of analytical methods in a pharmaceutical quality system: an overview focused on HPLC methods. *Quim Nova* 43:1190–1203. <https://doi.org/10.21577/0100-4042.20170589>
- [26] Brito NM, Amarante DEOP Jr, Polese L, Ribeiro ML (2003) Validação de métodos analíticos: estratégia e discussão. *Pestic Rev Ecotoxicologia e Meio Ambient* 13:129–146. <https://doi.org/10.5380/pes.v13i0.3173>
- [27] Polese L, Ribeiro ML (2003) Validação de métodos analíticos: estratégia e discussão. 129–146
- [28] Jeyabharathi C, Ahrens P, Hasse U, Scholz F (2016) Identification of low-index crystal planes of polycrystalline gold on the basis of electrochemical oxide layer formation. *J Solid State Electrochem* 20:3025–3031. <https://doi.org/10.1007/s10008-016-3228-1>
- [29] Vafaiee M, Vossoughi M, Mohammadpour R, Sasanpour P (2019) Gold-plated electrode with high scratch strength for electrophysiological recordings. *Sci Rep* 9:1–11. <https://doi.org/10.1038/s41598-019-39138-w>
- [30] Cherevko S, Topalov AA, Zeradjanin AR et al (2013) Gold dissolution: towards understanding of noble metal corrosion. *RSC Adv* 3:16516–16527. <https://doi.org/10.1039/c3ra42684j>
- [31] Marcel P (1974) Atlas of electrochemical equilibria in aqueous solutions, Second
- [32] Johnson D, Hilal N (2015) Characterisation and quantification of membrane surface properties using atomic force microscopy: a comprehensive review. *Desalination* 356:149–164. <https://doi.org/10.1016/j.desal.2014.08.019>
- [33] Holze R (2017) From current peaks to waves and capacitive currents: on the origins of capacitor-like electrode behavior. *J Solid State Electrochem* 21:2601–2607. <https://doi.org/10.1007/s10008-016-3483-1>
- [34] Abdinejad M, Santos da Silva I, Kraatz HB (2021) Electrografting amines onto silver nanoparticle-modified electrodes for electroreduction of CO₂ at low overpotential. *J Mater Chem A*. <https://doi.org/10.1039/d1ta00260k>
- [35] Wei H, Minghua W, Jufang Z, Zelin L (2009) Facile fabrication of multifunctional three-dimensional hierarchical porous gold films via surface rebuilding. *J Phys Chem C* 113:1800–1805. <https://doi.org/10.1021/jp8095693>

- [36] Li Y, Zhang L, Yang L et al (2021) Hydrolysis characteristics and risk assessment of a widely detected emerging drinking water disinfection-by-product: 2,6-dichloro-1,4-benzoquinone—in the water environment of Tianjin (China). *Sci Total Environ* 765:144394. <https://doi.org/10.1016/j.scitotenv.2020.144394>
- [37] Mortensen A, Granby K, Eriksen FD et al (2014) Levels and risk assessment of chemical contaminants in byproducts for animal feed in Denmark. *J Environ Sci Heal: Part B Pestic Food Contam Agric Wastes* 49:797–810. <https://doi.org/10.1080/03601234.2014.938546>
- [38] Qin F, Zhao YY, Zhao Y et al (2010) A toxic disinfection by-product, 2,6-dichloro-1,4-benzoquinone, identified in drinking water. *Angew Chemie: Int Ed* 49:790–792. <https://doi.org/10.1002/anie.200904934>
- [39] Shetti NP, Nayak DS, Malode SJ (2018) Electrochemical behavior of azo food dye at nanoclay modified carbon electrode—a nanomolar determination. *Vacuum* 155:524–530. <https://doi.org/10.1016/j.vacuum.2018.06.050>
- [40] Tran NH, Reinhard M, Gin KYH (2018) Occurrence and fate of emerging contaminants in municipal wastewater treatment plants from different geographical regions—a review. *Water Res* 133:182–207. <https://doi.org/10.1016/j.watres.2017.12.029>
- [41] Scholz F (2015) Voltammetric techniques of analysis: the essentials. *ChemTexts* 1:1–24. <https://doi.org/10.1007/s40828-015-0016-y>
- [42] Li Y, Liu Y, Liu J et al (2015) Molecularly imprinted polymer decorated nanoporous gold for highly selective and sensitive electrochemical sensors. *Sci Rep* 5:33–35. <https://doi.org/10.1038/srep07699>
- [43] Wang W, Qian Y, Boyd JM et al (2013) Halobenzoquinones in swimming pool waters and their formation from personal care products. *Environ Sci Technol* 47:3275–3282. <https://doi.org/10.1021/es304938x>
- [44] Zhao Y, Qin F, Boyd JM et al (2010) Characterization and determination of chloro- and bromo-benzoquinones as new chlorination disinfection byproducts in drinking water. *Anal Chem* 82:4599–4605. <https://doi.org/10.1021/ac100708u>
- [45] Du Y, Lv XT, Wu QY et al (2017) Formation and control of disinfection byproducts and toxicity during reclaimed water chlorination: a review. *J Environ Sci (China)* 58:51–63. <https://doi.org/10.1016/j.jes.2017.01.013>
- [46] Wang W, Qian Y, Jmaiff LK et al (2015) Precursors of halobenzoquinones and their removal during drinking water treatment processes. *Environ Sci Technol* 49:9898–9904. <https://doi.org/10.1021/acs.est.5b02308>
- [47] Ghosh A, Zhang C, Shi SQ, Zhang H (2019) High-temperature gas sensors for harsh environment applications: a review. *Clean: Soil, Air, Water*. <https://doi.org/10.1002/clean.201800491>
- [48] dos Santos Neto AG, de Sousa CS, da Silva FA et al (2018) Electrochemical sensor for detection of imipramine antidepressant at low potential based on oxidized carbon nanotubes, ferrocenecarboxylic acid, and cyclodextrin: application in psychotropic drugs and urine samples. *J Solid State Electrochem* 22:1385–1394. <https://doi.org/10.1007/s10008-017-3772-3>

Publisher's Note Springer Nature remains neutral with regard to jurisdictional claims in published maps and institutional affiliations.